Physical Properties of a New Deep Eutectic Solvent Based on a Sulfonium Ionic Liquid as a Suitable Electrolyte for Electric Double-Layer Capacitors

ARTICLE *in* THE JOURNAL OF PHYSICAL CHEMISTRY C · DECEMBER 2014

Impact Factor: 4.77 · DOI: 10.1021/jp5110455

2 AUTHORS, INCLUDING:

Mérièm Anouti
University of Tours
70 PUBLICATIONS **965** CITATIONS

SEE PROFILE

THE JOURNAL OF PHYSICAL CHEMISTRY C

Article

pubs.acs.org/JPCC

Physical Properties of a New Deep Eutectic Solvent Based on a Sulfonium Ionic Liquid as a Suitable Electrolyte for Electric Double-Layer Capacitors

Xiong Baokou and Mérièm Anouti*

Laboratoire PCM2E (EA 6296), UFR Sciences et Techniques, Université de Tours, Parc de Grandmont, 37200 Tours, France

Supporting Information

ABSTRACT: We present in this study the physical properties of two deep eutectic solvent (DES) mixtures based on solid sulfonium bis[(trifluoromethyl)sulfonyl]-imide (S_{111}TFSI) aprotic ionic liquid and two different H-bond donors, formamide (FMD) and trifluoroamide (TFA), according to temperature. First, we investigated their thermal properties by differential scanning calorimetry , and the results revealed the formation of a deep eutectic solvent giving a wide liquid range from −40 to 270 °C for these mixtures which froze at a much lower temperature than either of the individual components. The densities, ionic conductivities, and viscosities of these DESs were measured according to temperature and then discussed by applying Arrhenius or Vogel−Tamman−Fulcher (VTF) equations, as well as the Walden classification. Thanks to their favorable transport properties, both S_{111}TFSI/TFA and S_{111}TFSI/FMD mixtures contribute to the formulation of the electrolytes with 1 mol·L^{-1} LiTFSI. The performances of these electrolytes were then estimated by cyclic voltammetry, electrochemical impedance spectroscopy, and galvanostatic charge/discharge for activated carbon electrochemical double layer capacitor applications at 80 °C. The results showed that the selected H-bond donors allowed ion dissociation without solvation, increasing micropore accessibility and giving high capacitance values up to 350 F·g^{-1} in the case of formamide-based DESs. These unusual performances of the activated carbon material are debated with regards to the activation energy barrier to access the microporosity by ions in sulfonium-amides DESs.

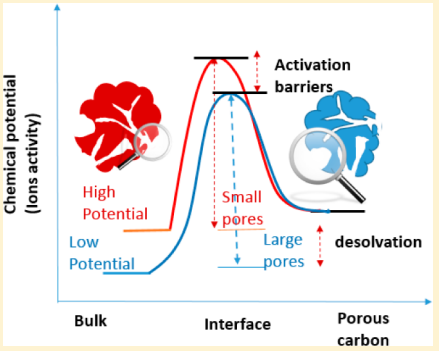

1. INTRODUCTION

Room temperature molten salts (RTMSs), also named ionic liquids (ILs), are only formed by ions and are liquid at ambient temperature. RTMSs are widely studied and used in a variety of electrochemical devices.[1−4] Recently reported as a subgroup of RTMSs, deep eutectic solvents (DESs) are ionic fluids formed by mixing salt and hydrogen-bond donors (H-BD), such as carboxylic acids, urea, or amides. In these complexes, the H-BD dissociate the salt's ions and shield the charge on the anion forming mixtures with a melting point much lower than either of the individual components.[5−11] Both ILs and DESs have gained much attention through their capability to induce versatile properties.[12]DESs have many properties in common with conventional ILs (e.g., nonreactive with water, nonvolatile, biodegradable, etc.), However, the most important property of DESs is their low cost of production, making them particularly desirable (more than ILs) for many large-scale applications in synthesis or as electrolytes for energy devices. Additionally, owing to their unexpected solvent properties as dissolvent for metal oxides, DESs can be tailor-made for large-scale applications as the electrowinning of metals from oxide matrices and stainless steel electropolishing.[11] Unfortunately, the potential application of DESs as electrolytes in energy storage devices has not been investigated in sufficient detail.

Electrochemical double layer capacitors (EDLCs or super-capacitors) are regarded as one of the most dependable electrochemical storage devices thanks to their high power and high-cycle life. These features make them appealing candidates for the development of advanced electric vehicles. Unfortunately for activated carbon (AC), the presence of micropores, inaccessible by the solvated ions in the electrolyte, limited the observation of the capacitance to its "theoretical" part, along with wetting deficiencies of electrolytes on the electrode surface, and/or the inability to successfully form a double layer in the pores. In this field, many studies are dedicated to improving the performance of the electrode materials (porosity, surface function, volumetric density, etc.).[13,14] However, the nature of the electrolyte is still fundamentally responsible for the limitations; in fact, the achievable cell voltage of supercapacitors depends considerably on the electrolyte breakdown voltage, while the equivalent series resistence (ESR) depends on the electrode and electrolyte conductivity. The choice of the electrolyte is therefore very influential. Currently, most used electrolytes are basic, acidic, or neutral aqueous solutions.[15−18] However, the main disadvantage of aqueous electrolyte-based supercapacitors is the restricted cell voltage and consequently, low energy.[19,20] Electrolytes based on organic solvent, are limited mainly by their environmental

Received: November 4, 2014
Revised: December 14, 2014

DOI: 10.1021/jp5110455
J. Phys. Chem. C XXXX, XXX, XXX−XXX

Table 1. Structure and COSMO Volume of Ions[26] in Formulated DESs

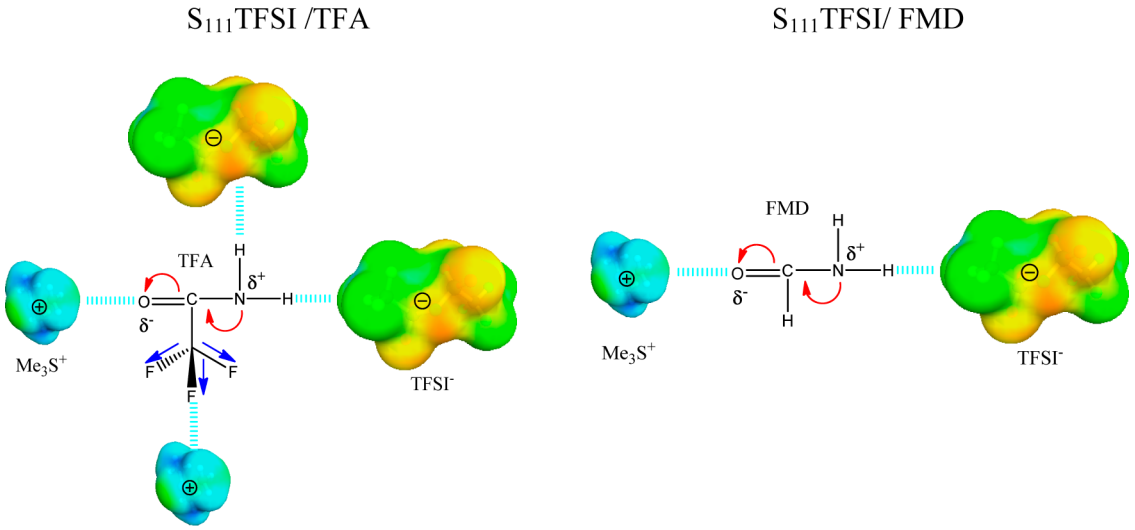

impact; those based on ILs are still restricted by their cost. Xu et al. reported studies on EDLCs based on AC with the lithium bis[(trifluoromethyl)sulfonyl]imide/acetamide deep eutectic system used as the electrolyte and revealed good specific capacity and rather good cycling performance, showing that these complex systems can be promising electrolytes for supercapacitors.[21,22] We have demonstrated in recent studies[6,23−25] that *N*-methylacetamide has the ability to form with lithium or sodium salt a deep eutectic solvent allowing the realization of lithium ion battery and EDLC devices that present promising performances of these electrolytes even at 80 °C. In the current work, new DESs constituted by mixing organic cation salts like trimethylsulfonium bis-[(trifluoromethyl)sulfonyl]imide [S_{111}][TFSI] ionic liquids which are solid at room temperature (T_m = 45 °C), were investigated with two different H-bond donor amides, specifically trifluoroacetamide (TFA) and formamide (FMD) as the electrolytes for EDLCs.

2. EXPERIMENTAL SECTION

2.1. Materials and DESs Preparation. Lithium bis-[(trifluoromethyl)sulfonyl]imide, (LiTFSI, ≥ 99.0%) was acquired from Solvionic. Trifluoromethylacetamide (TFA, 99.8%), formamide (FMD, 99%), and trimethylsulfonium iodide ([S_{111}][I], 99%) were purchased from Sigma-Aldrich. Trimethylsulfonium bis[(trifluoromethyl)sulfonyl]imide, (S_{111}TFSI) was obtained by ionic exchange from trimethyl iodide and LiTFSI as described in our previous work.[6,24,25] Equal quantities of dried S_{111}TFSI and amide (TFA or FMD), which are freshly distilled and degassed, were mixed at ambient temperature to prepare each DES solution until an uncolored fluid liquid is obtained. The DESs were stored in an Mbraun argon-filled glovebox. LiTFSI at 1 mol·L^{-1} was added to a corresponding volume of DES in order to formulate the studied electrolytes, thereby enabling a good conductivity. In this work, in each investigated electrolyte, coulometric Karl Fischer titration was used to determine the water content before and after any measurement. The values found were close to 300 ppm, denoted for each DES as S_{111}TFSI/TFA and S_{111}TFSI/FMD.

2.2. Methods. Density and viscosity measurements were carried out from 10 to 80 °C using an Anton Parr digital vibrating tube densitometer (model 60/602, Anton Parr, France) and an Anton Parr rolling-ball viscometer (model Lovis 2000M/ME, Anton Parr, France), respectively. The temperature in the cell was controlled within ±0.02 °C. The uncertainty of the density and viscosity measurements were 5 × 10^{-5}g cm^{-3}, and 1%, respectively.

The ionic conductivities were measured using a Crison (GLP 31) conductimeter. The temperature was controlled from 25 to 80 °C by a thermostated bath (JULABO F25) with an accuracy of ±0.2 °C. The calibration of the conductimeter was done using standard solutions of known conductivity (0.1 and 0.01 mol·L^{-1} KCl); the associated uncertainty did not exceed ±2%. Each conductivity was recorded when the stability was superior to 1% within 2 min. A PerkinElmer DSC 4000 was used under nitrogen atmosphere, coupled with an Intracooler SP VLT 100 to carry out differential scanning calorimetry (DSC) measurements. The samples were previously sealed in Al pans for DSC measurements.

Electrochemical measurements were carried out on a Versatile multichannel potentiostat (Biologic S.A). A Teflon Swagelok-type system with a two-electrode cell assembled in an argon-filled glovebox, with activated carbon as the working and counter electrodes and Whatman glass microfiber filter papers as separators, was used to conduct galvanostatic charge−discharge experiments and cyclic voltammograms (CVs). A thermostat allowed the control of the temperature with an accuracy close to 1 °C. Electrochemical impedance spectroscopy (EIS) measurements were conducted at an open circuit voltage (OCV) with a sinusoidal signal of 5 mV over the frequency range from 1 mHz to 100 kHz. The activated carbon electrode coated on aluminum foil (ϕ = 12 mm, with an active mass of 5.0 mg) was prepared with (polyvinylidene fluoride (PVDF) as binder (80 wt % AC, 10 wt % PVDF, 10 wt % carbon black) and was kindly supplied by Blue Solution, France.

3. RESULTS AND DISCUSSION

3.1. Physical Properties of the DES Electrolytes. The comparative behavior of both DESs is based on the different interactions between the two amides and ions in the sulfonium salt. These interactions affect both the physical properties of DESs and their performance as electrolytes during adsorption

DOI: 10.1021/jp5110455
J. Phys. Chem. C XXXX, XXX, XXX−XXX

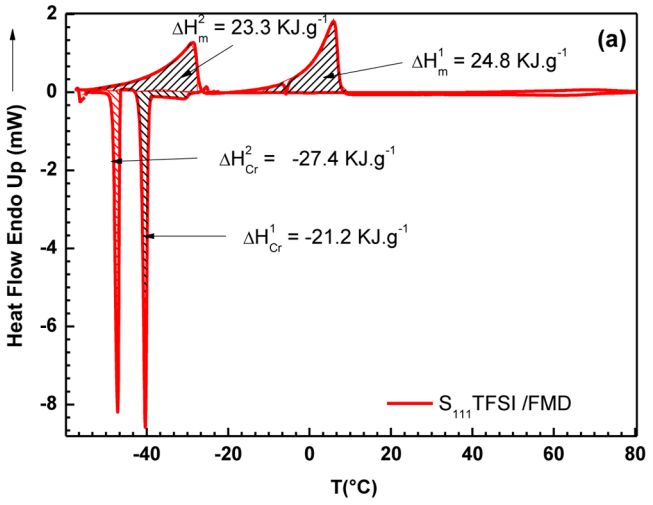

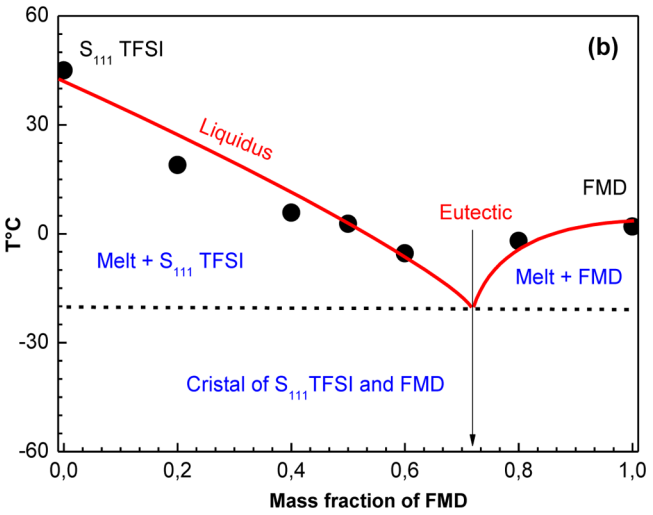

Figure 1. (a) Typical DSC curve of the S_{111}TFSI/FMD mixture for mass fraction of w(FMD) = 0.05 and (b) temperature−composition solid−liquid equilibrium diagram of the S_{111}TFSI/FMD binary system.

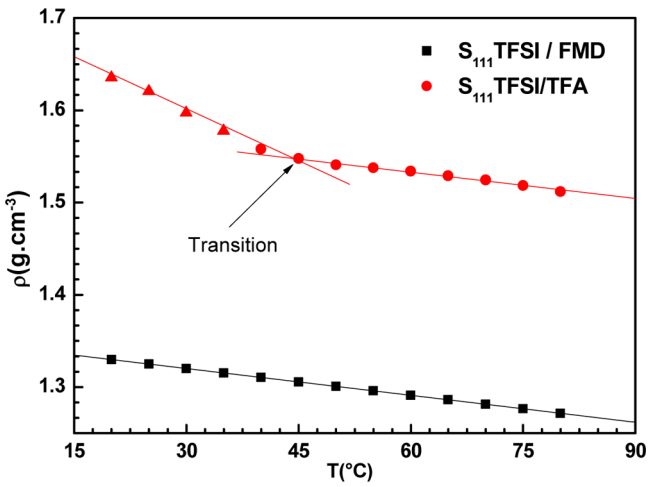

Figure 2. Dependence of densities (ρ) on temperature for sulfonium-based DESs with TFA amide red (●) and FMD amide black (■).

on AC. First, the withdrawing inductive effect of the trifluoromethyl group in TFA makes the H-bond interaction stronger, as well as the acid character of the amide group in

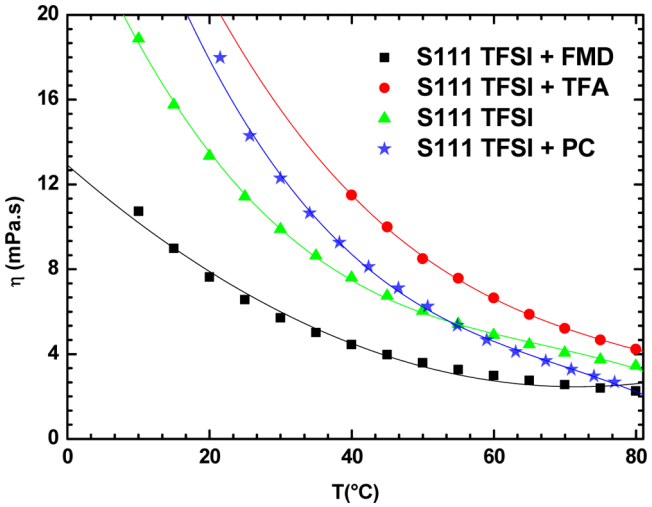

Figure 3. Evolution of the viscosity, η, of the sulfonium-based DESs with TFA amide and FMD amide according to temperature.

TFA, as shown in Table 1, through the expected structure of DES. Second, the presence of polar groups (C═O and NH_2 group) of amides enables the coordination with cations and anions, respectively. These interactions induce the breaking of the hydrogen bonds between amide molecules (TFA or FMD) and weakening of the Coulombic interaction between the $TFSI^-$ anions and the S_{111} or Li^+ cations in the salts. Hu et al.[27] showed the same behavior with DESs based on LiTFSI−urea or LiTFSI−acetamide mixtures. However, as the TFA structure is based on two polar groups (C═O and NH) and a trifluoromethyl group, the TFA molecules have stronger ion/solvent and solvent/solvent interactions in solution than acetamide or formamide.

3.1.1. Thermal Properties. As mentioned above, DESs are made by mixing two solids capable of generating a new liquid phase by self-association via hydrogen bonds. The general particularity of this new phase is the lower freezing point than that of initial, individual constituents. Figure 1a shows a typical thermogram for the studied DESs, obtained by DSC curves between −60 and 100 °C (shown here for the S_{111}TFSI/FMD system; $w_{(FMD)}$ = 0.5). Figure 1b shows the temperature−composition solid−liquid equilibrium diagram of the S_{111}TFSI/FMD binary systemobtained from the DSC thermograms for all mass fractions ($0 < w_{(FMD)} < 1$).

Usually, to characterize the eutectic composition and temperature of DESs, the freezing temperature at which the first solid starts needs to be established in order to create a cooling diagram depending on the composition. The majority of the systems become solid on freezing and the exact freezing point is difficult to identify. For instance, when FMD and S_{111}TFSI IL are mixed together, the freezing point of the eutectic solution is −40 °C, which is considerably lower than the melting point of S_{111}TFSI and FMD (45 and 2.5 °C, respectively).

In Figure 1, two endothermic peaks, representing the typical behavior of an eutectic can be observed in the sample, showing the liquid−solid coexistence regime between −50 and 7 °C. The presence of two peaks is attributed to the intrinsic plastic crystal behavior of the sulfonium TFSI salt, as we demonstrated in our previous work by the pure sulfonium salt thermogram.[28] Beyond 100 °C, both compounds are stable up to 210 °C (FMD) and 250 °C (S_{111}TFSI). The DSC thermograms of all

DOI: 10.1021/jp5110455
J. Phys. Chem. C XXXX, XXX, XXX−XXX

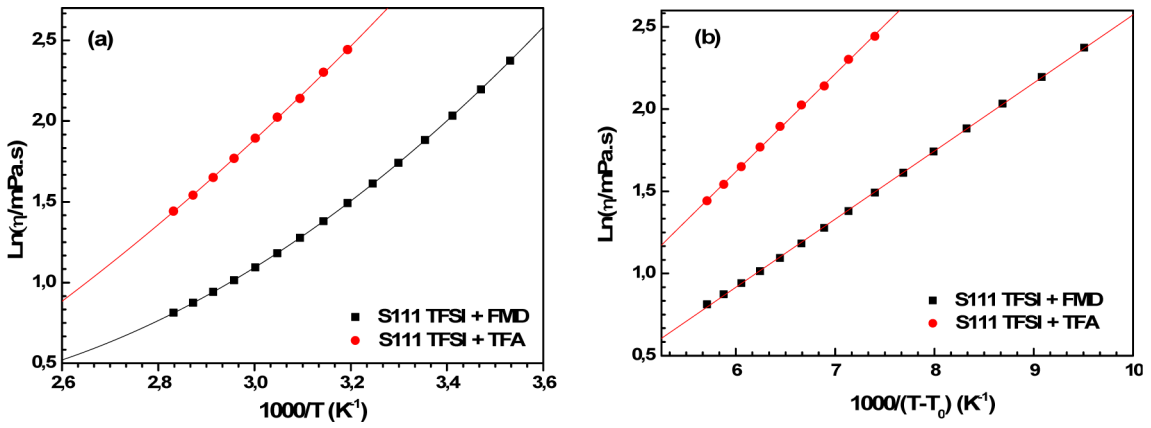

Figure 4. Fitting curves of viscosity, η, according Arrhenius-low (a) and VTF-equation (b) of the sulfonium-TFA (red ●) and sulfonium-FMD (black ■) DESs.

Table 2. Fit Parameters from VTF Equation for the Conductivity and the Viscosity Temperature-Dependence (T_0, σ_0, η_0, $R{\cdot}B_{\eta,\sigma}$) of the S_{111}TFSI/H-BD System

VTF equation parameters	system	T_0 (K)	η_0 (mPa·s) or σ_0 (mS·cm^{-1})	$R{\cdot}B_{\eta,\sigma}$ (J mol^{-1})	R^2
conductivity	S_{111}TFSI/FMD	179	398	3.17	0.9994
	S_{111}TFSI/TFA	175	699	4.59	0.9998
viscosity	S_{111}TFSI/FMD	182	0.228	3.24	0.9999
	S_{111}TFSI/TFA	178	0.141	4.95	0.9994

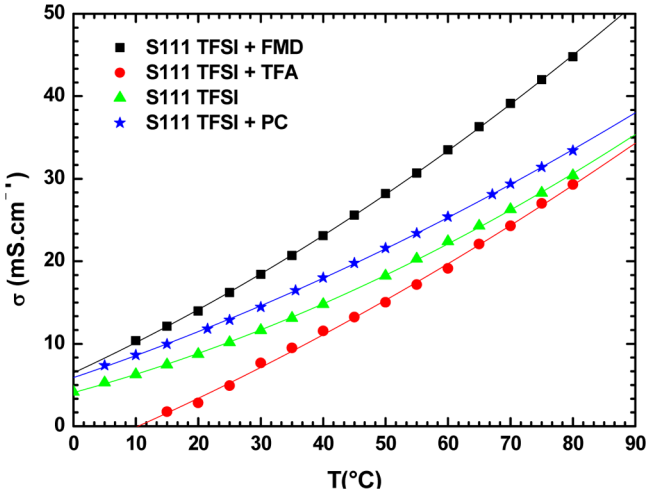

Figure 5. Influence of temperature on the conductivity of the sulfonium based DESs in mixture with TFA, FMD, PC, and for pure S_{111}TFSI. The solid line serves as a guide to the eye.

compositions (Figure 1S in Supporting Informations) allow the building of the temperature−composition solid−liquid equilibrium diagram of the S_{111}TFSI/FMD binary as shown in Figure 1b, and the deduction of the eutectic characteristics (w_e = 0.71 ; T_e = −20 °C).

3.1.2. Density. The DESs densities were measured over the temperature range of 20 to 80 °C and atmospheric pressure. As displayed in Figure 2, TFA-based DES has a higher density than its counter parts with FMD due to a higher intermolecular packing of the compound (ρ = 1.328 for DES based on FMD and 1.633 on TFA).

The strong interaction due to the trifluoromethyl group could be the reason behind the difference in density observed, since this group is widely responsible for a more compact volume in the case of S_{111}/TFA. The densities of both DESs are superior to those of pure HBDs (TFA, 1.16; FMD, 1.32 g cm^3). As expected in general, the density measured for both DESs revealed a linear decrease with temperature: indeed, as a result of the thermal expansion, substances (at constant pressure) become less dense while the temperature increases. Furthermore, Figure 2 reveals a break in the slope at T = 45 °C for the TFA-based mixture that we could attribute to an easy phase transition occurring on the trimethylsulfonium cation as shown for pure sulfonium IL, which demonstrates plastic behavior.[28,29] Beyond this temperature, both mixtures have the same slope for $\rho = f(T)$ (variation). The density values obtained for S_{111}TFSI/TFA were higher in comparison to those reported by Abbot et al.[30] in the case of TFA and ammonium chloride, ρ = 1.342 for ($EtNH_3Cl$/TFA) or (cholinium chloride/TFA) with ρ = 1.273 g·cm^{-3}.

3.1.3. Dynamic Viscosity. The free volume and the probability of finding holes of suitable dimensions into which the species can move[31−35] determine the viscosity of a fluid. The relatively high viscosity of ionic liquids can be explained by the relatively large radii of ions that are found to be several times higher than the average radius of the voids. It is important to wisely choose the solvent and salt since they generally highly and strongly affect the viscosity of the DESs, because that feature is driven by structures of the DESs, which determine the nature of intermolecular interactions occurring between the amide molecules and ions in solution. For example, as presented in Figure 3, the TFA-based DES shows a viscosity about three times higher at 40 °C (4 mPa·s and 12 mPa·s for S_{111}TFSI/FMD and S_{111}TFSI/TFA, respectively). Nevertheless, for the pure ILs S_{111}TFSI and (S_{111}TFSI, + propylene carbonate (PC)) mixture, the viscosities η = f(T) are intermediate in the whole temperature range.[26,28] As shown in Table 1 the strong interactions between the sulfonium cation and the trifluoro-group and carbonyl group, as well as between the amide hydrogen and the $TFSI^-$ anions, are mainly responsible for these last observations. As a consequence, in

DOI: 10.1021/jp5110455
J. Phys. Chem. C XXXX, XXX, XXX−XXX

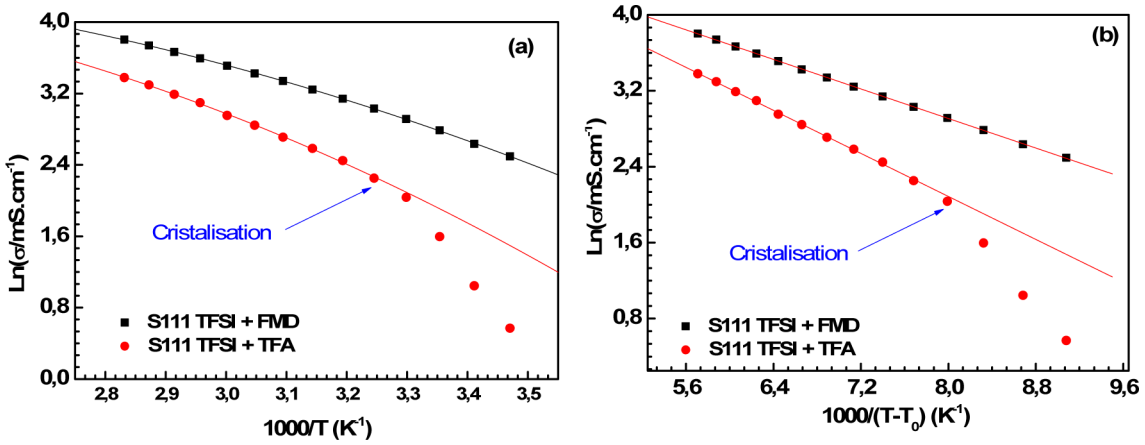

Figure 6. Arrhenius (a) and VTF (b) plots of the ionic conductivity temperature-dependence of the sulfonium-based DESs in mixture with trifluoroacetarmide (TFA) (red ●) and formamide (FMD) (black ■).

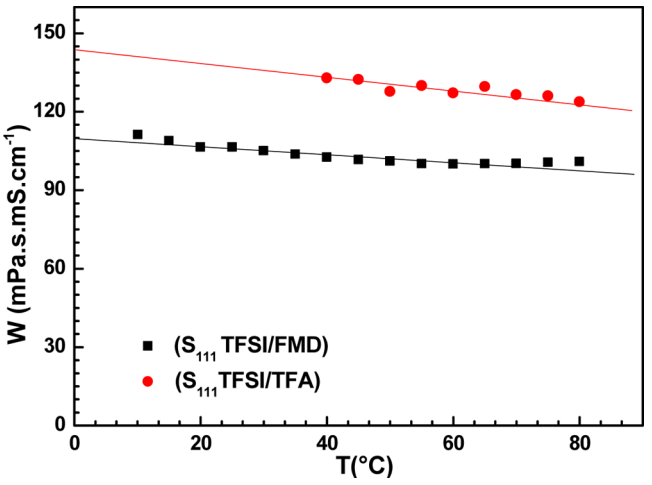

Figure 7. Walden $\sigma\eta$ of the sulfonium-based DESs in mixture with TFA (red ●) and FMD (black ■). The solid line is the "ideal" Walden product line fixed with 1 mol·L^{-1} aqueous KCl solutions.

the case of TFA-based DESs the dissociation of ions and the strong interactions from the H-bond donor-induced packing by molecular organization decreases the void's volume, thus leading to a drastic increase in viscosity and density.

Moreover, according to Figure 3, the viscosity (η) for both DESs diminishes logically while the temperature augments from 10 to 80 °C. The change in viscosity, η, with temperature is portrayed by $\eta = \eta_0 \exp[E_a^{\eta}/(RT)]$ if the viscosity obeys the Arrhenius' Law, otherwise the Vogel−Tamman−Fulcher equation (VTF) is followed. This equation can serve to fit the dependence $\eta = f(T)$. Fitted curves of viscosity according to temperature for S_{111}TFSI/H-BD DESs are shown in Figure 4. As can be seen, the Arrhenius plot (Figure 4a) has a curved profile, pointing out the fact that the ionic viscosity temperature-dependence of both DESs mixture does not obey the Arrhenius' Law. In this case the temperature-dependence fit according VTF equation $\eta = \eta_0 \exp[B_\eta/(T - T_0)]$ is applied with success as demonstrated in Figure 4b, which implies a solvent-assisted viscous flow mechanism. We may be able to explain the variation in viscosity during the temperature increase by a decrease in interaction in the mixture between the $TFSI^-$ anion and the H-BD[36] driven by the hydrogen bonds.

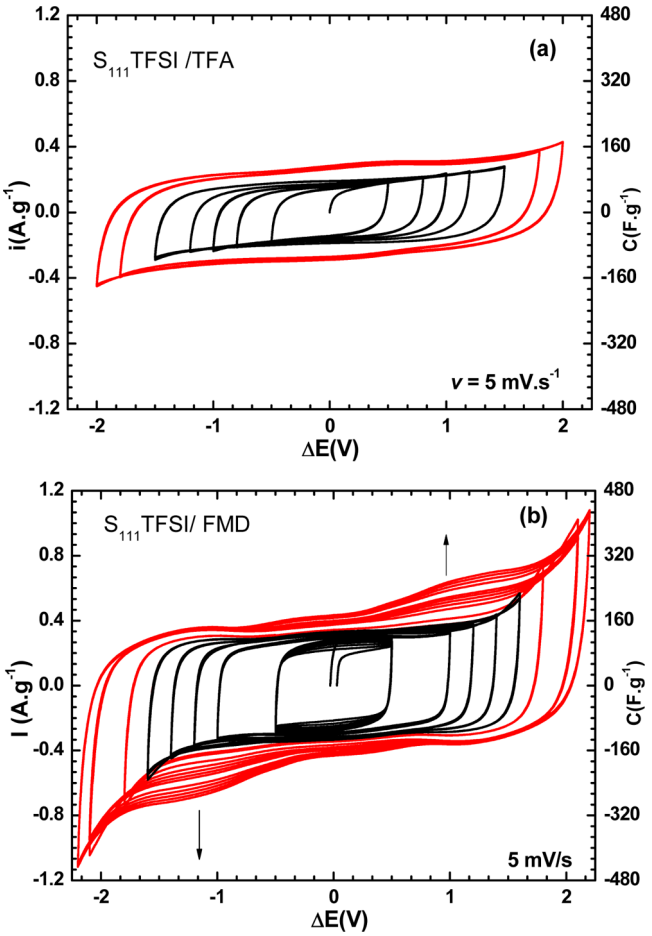

Figure 8. CV curves of AC-based EDLCs of the sulfonium-based DESs in mixture with TFA (a) and FMD (b) between 0 and 2.2 V at a scan rate v = 5 mV·s^{-1} and T = 80 °C.

Table 2 shows the best VTF fitting parameters from the VTF equation, η_0 (mPa·s), B_η (K), and T_0. These values are comparable with other DESs and ionic liquids.[6,24,25,37] Fluorination of the H-BD leads to a decrease in the E_η value, as predicted by the "hole" theory. On the basis of this theory, Abbott et al.[38] commented that the availability of holes large enough for the mobile species to enable their insertion limits the viscosity of fluids. Larger H-BD molecules like TFA raise

DOI: 10.1021/jp5110455
J. Phys. Chem. C XXXX, XXX, XXX−XXX

Table 3. Capacitances of EDLCs of the Sulfonium-Based DESs in Mixture with Trifluoroacetarmide (TFA) (a) and Formamide (FMD) (b) between 0 and 2.2 V at 5 mV·s^{-1} scan rate; T = 80 °C

	specific capacitance (F·g^{-1})	
ΔE (V)	S_{111} TFSI +TFA	S_{111} TFSI + FMD
0.5	106	195
1.0	126	214
1.5	147	277
1.8	200	286
2.0	214	357

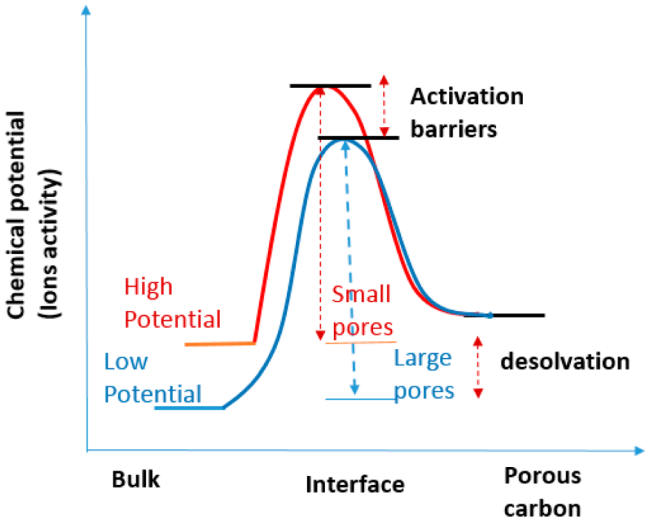

Figure 9. Schematic illustration of the kinetic barrier for ion transfer crossing the small or large pores in the carbon/electrolyte interface in relation to high or low applied potential producing ion desolvation.

the ionic radius of the DES complex, which reduces the free volume and consequently increases viscosity and density.

3.1.4. Conductivity. The evolution of the conductivity of both DES mixtures according to the temperature from 10 to 80 °C as well as the equivalent mixture of S_{111}TFSI with propylene carbonate (PC) and a pure solution of S_{111}TFSI for comparison are related in Figure 5. As anticipated, the conductivity of the solution increases gradually with the temperature. For example, the conductivity of these solutions is close to 3.01 mS·cm^{-1} and to 14.4 mS·cm^{-1} at 20 °C, and reaches 25 mS·cm^{-1} and 46 mS·cm^{-1} at 80 °C for the S_{111}TFSI/FMD and S_{111}TFSI/TFA mixtures, respectively. For the overall temperature range, FMD-based DES is more conductive than the one based on TFA S_{111}TFSI/FMD, which is three time higher than S_{111}TFSI/TFA at 25 °C.

This difference in conductivity may be due to the lower mobility of the sulfonium cation in solutions with TFA because of its interaction with the fluorine group (Table 1). When compared with pure S_{111}TFSI, it appears that the high dissociation capability allows better ionic mobility and thus a higher conductivity of formamide (ε = 109) than that of TFA. On the other hand, the much stronger H-bond donor effect of the trifluoroacetate group in TFA weakens the ionic mobility of ions, especially at low temperature.

In comparison, when a dissociating solvent like PC is added, the ionic mobility also slightly increases, but is held back by the solvation of ions with PC; the effect of temperature is then less pronounced. In electrolytic solutions, the mobility of the ions is dependent upon not only on the size of the voids, but also on the size of the migrating species and the radii of the cations and complexed anions. In the present case, the presence of TFA promotes a void, but the size of the complexed ions disadvantages their mobility. At the same time, dissociation without solvation of ions in the H-bond donor is an advantage in the EDLC application to access microporosity.

The ionic conductivity temperature-dependence of the S_{111}TFSI/amides DESs reviewed was then investigated by regressing the data to an Arrhenius-like equation $\sigma = \sigma_0 \exp[E_a^\sigma/(RT)]$ and VTF-like equation $\sigma = \sigma_0 \exp[B_\sigma/(T - T_0)]$ from 10 to 80 °C. The curves obtained are shown in Figure 6. Regarding the viscosities values, only the VTF form fits the $\sigma = f(T)$ correctly.

Table 2 shows all VTF equation parameters for the conductivity temperature-dependence (T_0 (K), σ_0 (mS·cm^{-1}), B_σ (K)) of S_{111}/FMD and S_{111}/TFA. $B_{\eta,\sigma}$ can be linked to the energy barrier that needs to be overcome for the species in the DES to move past each other. Moreover, its value can be linked to the salt structure and HBD molecule.[39] In other word, the smaller are the $B_{\eta,\sigma}$ values, the easier it is for the ions to move

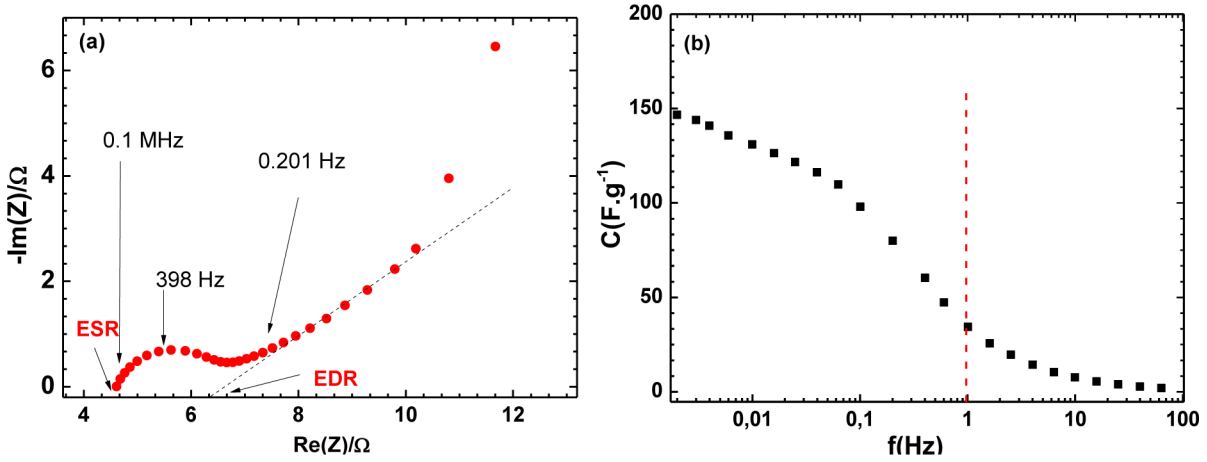

Figure 10. EIS spectra in the open circuit tension of the positive AC electrode in three electrode cells recorded at 80 °C in the frequency ranging from 100 kHz to 10 mHz for the sulfonium-based DESs in a mixture with FMD as the electrolyte: (a) Nyquist plots; (b) impedance frequency-capacitance correlation.

DOI: 10.1021/jp5110455
J. Phys. Chem. C XXXX, XXX, XXX−XXX

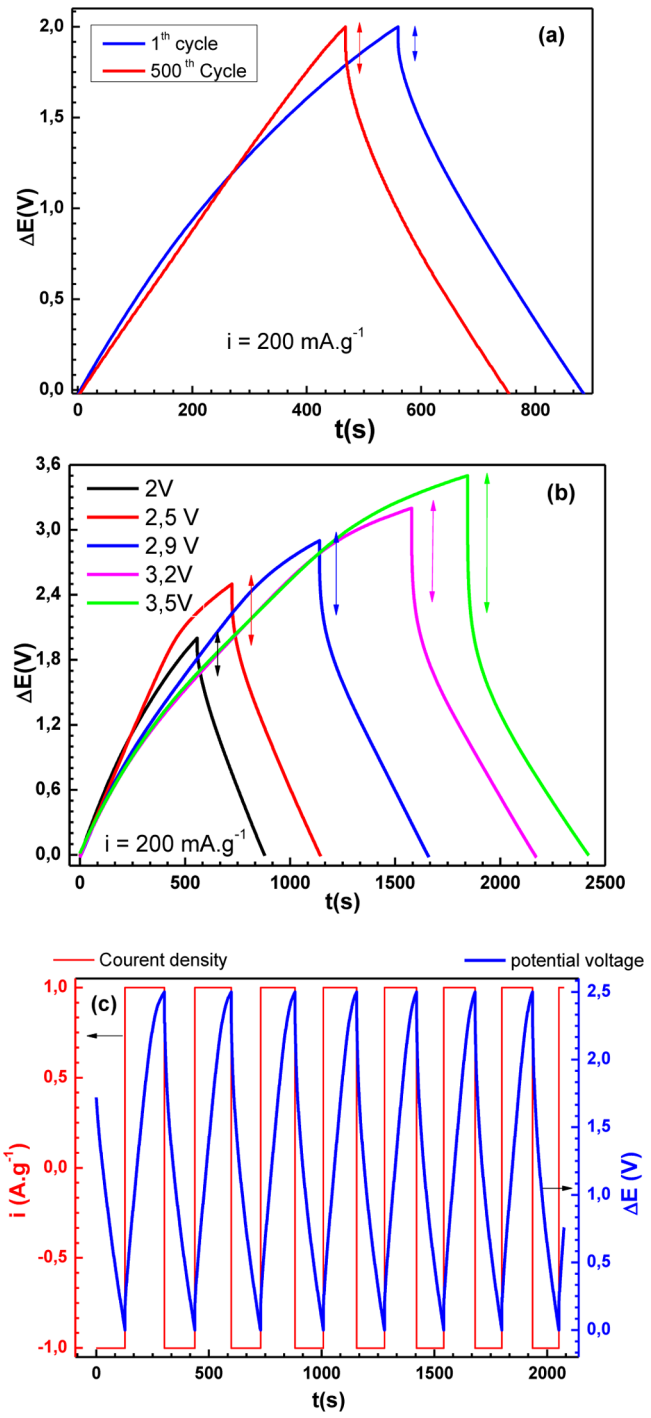

Figure 11. Galvanostatic charge/discharge on the activated carbon electrode with S_{111}TFSI/TFA as the electrolyte (T = 80 °C): (a) current density of 1 A·g^{-1} and applied tension of ΔE = 2.5 V; (b) for various tension voltages (i.e., 2.0, 2.5, 2.9, 3.2, and 3.5 V) at a current density of 200 mA·g^{-1}; (c) cycling at ΔE = 2.5 V and I = 1 A·g^{-1} on long-time cycling (1000 cycles).

Table 5. Specific Capacitance, Specific Energy, and Specific Power for the S_{111}TFSI+FMD at 80 °C (ΔV = 2.2 V) at the Specified Cycle Number

	1	300	600	800	1000
C_{sp} (F·g^{-1}) (I = 0.25A·g^{-1})	280	258	254	231	227
C_{sp} (F·g^{-1}) (I = 5 A·g^{-1})	135	121	118	113	108

past each other, and the lower the viscosity is in the solution. The good concordance between the activation energies for ionic conductivity and viscosity ($B_\eta \approx B_\sigma$) may imply that electrostatic forces, which enhance the ionic conduction, are more predominant in these DES systems than van der Waals interactions, which determine the level of fluidity of the solution.

3.1.5. Ionicity of DES Mixtures. To evaluate the ionicity of ILs, RTMSs, or DESs we can use the Walden product related to the classical Walden rule.[40,41] The product of the normalized conductivity σ by the fluidity η^{-1} is called the Walden product and relates the ionic mobility of the medium through which the ions move. Figure 7 shows the variation of $W = \sigma\eta$ at various temperatures from 10 to 80 °C in the case of S_{111}+FMD and S_{111}+TFA.[42] The constant value of W with temperature is observed for mobile ions and only relies on the viscosity of the medium and the number of ions present in the equivalent volume that is indicated by the salt composition; that is, all ions contribute equally to the conductivity. This feature corresponds to either an ideal solution or to an infinite dilution in the absence of any interaction.

The results obtained in Figure 7 indicate that the ionicity of the DESs studied is sensitive to temperature. W decreases when temperature increases; the medium becomes then more "ionic" according to the Walden classification. This observation can be linked, as discussed above, to the low energy of the viscous flow value associated with this solution, which further suggests the better characteristic of this mixture for use as an electrolyte for energy storage applications.

3.2. Evaluation of EDLC Performance at the AC Electrode. It is well-known that the rectangular shape of the voltammetry characteristics express the ideal capacitance behavior of a carbon material electrode.

Figure 8 shows the cyclic voltammetry (CV) curve recorded with AC as the electrode in a symmetric system with S_{111}TFSI/TFA (a) and S_{111}TFSI/FMD (b) used as electrolytes at 80 °C and a scan rate of v = 5 mV·s^{-1}. The curves are expressed by the current density (A·g^{-1}) and capacitance in F·g^{-1} represented on the same scale in all the tested potential ranges, for comparison.

At first, it can be seen that despite the relatively high viscosity ($2.5 < \eta < 4$) mPa·s at 80 °C in comparison to a classical, acidic aqueous solution ($\eta \approx 0.8$ mPa·s) or an organic solution, acetonitrile for example ($\eta \approx 0.3$ mPa.s^{-1}), both systems display a rectangular-shaped CV, which is typical for EDLC; the more rectangular curve in the case of S_{111}TFSI/FMD (Figure 8b) reveals better ion propagation. For the potential voltage, $\Delta E > 1.8$ V, the current leap is essentially attributed to more ion storage. Table 3 shows the specific capacitance calculated from the CVs as $(2\int idt)/(m\cdot\Delta E)$ according to the applied

Table 4. Specific Capacitance, Specific Energy, and Specific Power for the S_{111}TFSI+TFA DES at 25 °C (I = 200 mA·g^{-1})

	ΔV = 2.0 V	ΔV = 2.5 V	ΔV = 2.9 V	ΔV = 3.2 V	ΔV = 3.5 V
C_{sp} (F·g^{-1}) at 1st cycle	144	107	124	145	148
C_{sp} (F·g^{-1}) at 20th cycle	115	108	127	132	128

DOI: 10.1021/jp5110455
J. Phys. Chem. C XXXX, XXX, XXX−XXX

potential ΔE from 106 to 214 F·g^{-1} for S_{111}TFSI/TFA and from 219 to 357 F·g^{-1} for S_{111}TFSI/FMD. The super capacitive behavior promoted by the microporosity (pore size, 0.7 nm < Ø <1.2 nm) of the carbon used is correlated to the reduction of Van der Walls repulsion toward the electrostatic interactions when the electrode polarization is increased. Furthermore, for low applied tension, the ions access near the electrode surface and in large pores, while for higher tension, ions access (or depart from) more active sites in the carbon.

The weakly bound complex S_{111}/H-BD easily desolvated, transcribes a more complete charge accumulation (or depletion) in the electrode, and hence a better capacitive current. The presence of an amide at the carbon surface is likely to affect this behavior as well, which participates positively in the double layer thanks to the exceptional dielectric constant values (ε_r = 109 for FMD) involved in the capacitance, as expected by the double-layer capacitance equation: $C_{dl} = \varepsilon_0\varepsilon_r/d$ where ε_0 and ε_r are the dielectric constants of the vacuum and the electrolytic medium, respectively. In other words, the energy necessary to access carbon microporosity must overcome the ion desolvation energy. This energy may be sufficient when electrode polarization increases by raising the applied potential. At the same time, the decomposition of the electrolyte may be reached if the stability limit of the electrolyte (and/or material) is attained, that is, at high potential.

Here, the small pores are not accessible to ions and only a partial surface area is accessible. In summary, two conditions are necessary for ion accessibility into the microporosity: (i) low energy solvation of ions and (ii) electrochemical stability of the electrolyte above the electrochemical activation limits, that is, polarization necessary for desolvation. Figure 9 illustrates the activation barriers to access the meso- and microporosity in connection with the ion-desolvation energies. For given potential and ions, the energy barrier associated with the insertion in small pores is higher than with insertion in large pores. Nevertheless, if we consider both a different size of pores and a different potential, the difference between the two barriers on both curves is then the same.

The very high and unusual capacitance values observed in the case of DMF and to a lesser extent TFA, are not so surprising if we consider the observations of Bedrov and Gogotsy's groups,[18] which investigated through simulations the non-Faradaic capacitance enhancement that can be obtained in the nanoporous electrode by systematic comparison of the various shapes and dimensions. A noticeable improvement in the capacitive storage is observed when the electrode curvature and the length scale of the surface roughness with spacing ranging between 6.6 and 8.0 Å are comparable to ion dimensions. Their results show that nanoconfinement can generate non-Faradaic capacitance ranging from 260 to 350 F/g, which significantly exceeds the performance of the current generation of nanostructured electrodes. In this study, the capacity to desolve lithium, TFSI, and sulfonium ions can provide the same nanoconfinement giving capacitances ranging from 200 to 357 F·g^{-1} for S_{111}TFSI/FMD.

3.2.1. Electrochemical Impedance Spectroscopy (EIS) on Two-Electrode Cells. In general, we can observe by electrochemical impedance spectroscopy (EIS) tree domains in the Z'' = $f(Z')$ Nyquist plot of an EDLC: (i) the contact resistance between the active material and the current collector is represented by a semicircle at high frequencies; the equivalent resistance (sum of resistances of active material, current collectors, the electrolyte in the separator, and contact resistance) is the value obtained at $\omega \to \infty$; (ii) the Warburg region, which corresponds to the middle-frequency region, represented by a 45° line, is rather due to frequency-dependent resistance $R(\omega)$ associated with the ionic resistance in the porosity;[43] (iii) a quasi-vertical line in the low-frequency region reflects the purely capacitive phenomena;[44] the associated resistance, named equivalent diffusion resistance (EDR), results from the intercept of the line with the Z' axis.

Figure 10a presents the Nyquist plots in the frequency ranging from 100 kHz to 10 mHz for the positive AC electrode in a supercapacitor assembled with three-electrode cells recorded at 80 °C with S_{111} TFSI/FMD as the electrolyte before cycling. An exploitation of Figure 10a reveals a relatively small Warburg region indicating low ion diffusion impedance, driving a lower obstruction of the ion movement and a better charge propagation in the mesoporous carbon for the formation of double layers. The experimental ESR read on the figure (ESR = 4 Ω) is higher than the classical aqueous solution (ESR = 0.5 Ω) which is expected given the relatively low ionic conductivity of amide DESs. At the same time, high EDR values indicate high-ionic resistance in the carbon porosity, which highlights the difficult insertion of anions into the porosity of the activated carbon electrode in the open circuit (ΔE = 0 V) induced by differences in ion volumes (e.g., V_{COSMO}(TFSI) = 219.4 Å^3; $V_{COSMO}(S_{111})$ = 56.7 Å^3) (Table 1).[24,26] The low frequency impedance is correlated to capacitance by $C_S = 1/(2\pi f Z'' m)$, where f is the frequency and Z'' is the imaginary component of the impedance. As expected in the lowest frequency at 0.10 Hz, only mesoporosity-adsorption capacitance close to 150 F/g is observed, that particular region being sufficiently low to solely witness the only capacitive behavior of the carbon (Figure 10b).

3.2.2. Galvanostatic Charge–Discharge on Two-Electrode Cells. Galvanostatic charge/discharge experiments were realized with various tension voltages ranging between 2 and 3.5 V at 200 mA·g^{-1} and for a current density of 1 A·g^{-1} in order to further investigate electrolyte performance.

Figure 11a displays an example of charge–discharge curves of two-electrode cells with active carbon on S_{111}TFSI/TFA at the first and 500th cycle. Figure 11b shows the charge/discharge curve for various tension voltages (i.e., 2.0, 2.5, 2.9, 3.2, and 3.5 V) at a current density of 200 mA·g^{-1}. Figure 11c shows cycling at ΔE = 2.5 V and I = 1 A·g^{-1} on long-time cycling (1000 cycles). Figure 11a shows that after several cycles, the charge/discharge curve approaches the triangular shapes reflecting a more conventional capacitive behavior when ions adsorb to the accessible surface. The specific capacitance (C_{sc}) was determinate by using $C_{sp} = 2I\Delta t/(m\Delta V)$, at discharge cycle. Here, I is the constant discharge current, ΔV is the voltage drop upon discharge (excluding the resistance IR drop), Δt is the discharge time, and, m is mass of the one electrode. Values of specific capacitance, derived from the AC electrode in the galvanostatic mode, are presented in Table 4 and Table 5. Figure 11b shows the increasing IR drop when increasing the applied tension in the symmetric system. The interface resistance and ion migration resistance in the electrode are mainly responsible for this potential drop. This behavior may be caused by the difficulty of the anions to access the positive electrode's microporosity, which limits the charging system. Similar behavior can be seen in the electrochemical activation by a voltage-driven, ion intercalation process, during which ion-accessible sites are abundantly created, and can be used for mixed ion adsorption/intercalation charge storage. Similar

DOI: 10.1021/jp5110455
J. Phys. Chem. C XXXX, XXX, XXX–XXX

behavior was shown by Zhang et al.,[45] demonstrating the solvents, and applied voltage effects, and cation selection on ions intercalation behavior using galvanostatic charge−discharge. In our study, for an applied tension of 2.5 V and a current density of 1 $A{\cdot}g^{-1}$, the discharge curves show a poor capacity retention of less than 80% (Figure 11c and Table 5), indicating pore obstruction when the applied tension and current density is increased.

4. CONCLUSIONS

To answer the problems caused by the presence of micropores, inaccessible to the solvated ions in the electrolyte and/or the unsuccessful formation of a double layer in the pores, two sulfonium-based DES electrolytes were characterized through their thermal and transport properties. A number of suitable properties were reported, for exampe, ionic character, wide liquid phase, and high-ionic conductivity up to 28.4 $mS{\cdot}cm^{-1}$ and 45 $mS{\cdot}cm^{-1}$ at 80 °C for S_{111}TFSI/FMD and S_{111}TFSI/TFA, respectively, which demonstrated that these DESs can be used as an electrolyte for supercapacitors. Through the testing of their electrochemical performances for EDLC use as electrolytes using AC electrodes, a comparative evaluation was established. The results revealed that EDLC using S_{111}TFSI/H−B DES as an electrolyte can be charged up to 2.5 V with a capacitance of the AC electrode close to 350 $F{\cdot}g^{-1}$ driven by high dissociation and the weak H-bond complex formed. In light of these results, the conditions needed for better micropore accessibility of ions are discussed according to the energy solvation of ions and the activation barriers to access the meso- and microporosity.

■ ASSOCIATED CONTENT

Supporting Information

DSC of the S111TFSI/FMD mixtures for mass fraction of $0 < w_{(FMD)} < 1$. This material is available free of charge via the Internet at http://pubs.acs.org

■ AUTHOR INFORMATION

Corresponding Author

*E-mail: meriem.anouti@univ-tours.fr. Fax: (33)247367360. Tel: (33)247366951.

Notes

The authors declare no competing financial interest.

■ ACKNOWLEDGMENTS

This research was supported by an initiative academic region project. The authors thank Blue Solution (France) for providing the carbon electrode materials.

■ REFERENCES

(1) Ho, T. D.; Zhang, C.; Hantao, L. W.; Anderson, J. L. Ionic Liquids in Analytical Chemistry: Fundamentals, Advances, and Perspectives. *Anal. Chem.* **2013**, *86*, 262−285.

(2) Zhang, S.; Miran, M. S.; Ikoma, A.; Dokko, K.; Watanabe, M. Protic Ionic Liquids and Salts as Versatile Carbon Precursors. *J. Am. Chem. Soc.* **2014**, *136*, 1690−1693.

(3) Lu, X.; Burrell, G.; Separovic, F.; Zhao, C. Electrochemistry of Room Temperature Protic Ionic Liquids: A Critical Assessment for Use as Electrolytes in Electrochemical Applications. *J. Phys. Chem. B* **2012**, *116*, 9160−9170.

(4) Chakrabarti, M. H.; Mjalli, F. S.; AlNashef, I. M.; Hashim, M. A.; Hussain, M. A.; Bahadori, L.; Low, C. T. J. Prospects of Applying Ionic Liquids and Deep Eutectic Solvents for Renewable Energy Storage by Means of Redox Flow Batteries. *Renew. Sustain. Energy Rev.* **2014**, *30*, 254−270.

(5) Abbott, A. P.; Capper, G.; Davies, D. L.; Rasheed, R. K.; Tambyrajah, V. Novel Solvent Properties of Choline Chloride/Urea Mixtures. *Chem. Commun.* **2003**, 70−71.

(6) Zaidi, W.; Boisset, A.; Jacquemin, J.; Timperman, L.; Anouti, M. Deep Eutectic Solvents Based on *N*-Methylacetamide and a Lithium Salt as Electrolytes at Elevated Temperature for Activated Carbon-Based Supercapacitors. *J. Phys. Chem. C* **2014**, *118*, 4033−4042.

(7) Abbott, A. P.; Azam, M.; Ryder, K. S.; Saleem, S. In Situ Electrochemical Digital Holographic Microscopy; A Study of Metal Electrodeposition in Deep Eutectic Solvents. *Anal. Chem.* **2013**, *85*, 6653−6660.

(8) Dai, Y.; van Spronsen, J.; Witkamp, G.-J.; Verpoorte, R.; Choi, Y. H. Ionic Liquids and Deep Eutectic Solvents in Natural Products Research: Mixtures of Solids as Extraction Solvents. *J. Nat. Prod.* **2013**, *76*, 2162−2173.

(9) Paiva, A.; Craveiro, R.; Aroso, I.; Martins, M.; Reis, R. L.; Duarte, A. R. C. Natural Deep Eutectic Solvents—Solvents for the 21st Century. *ACS Sustain. Chem. Eng.* **2014**, *2*, 1063−1071.

(10) Abbott, A. P.; Boothby, D.; Capper, G.; Davies, D. L.; Rasheed, R. K. Deep Eutectic Solvents Formed between Choline Chloride and Carboxylic Acids: Versatile Alternatives to Ionic Liquids. *J. Am. Chem. Soc.* **2004**, *126*, 9142−9147.

(11) Abbott, A. P.; Capper, G.; Davies, D. L.; McKenzie, K. J.; Obi, S. U. Solubility of Metal Oxides in Deep Eutectic Solvents Based on Choline Chloride. *J. Chem. Eng. Data* **2006**, *51*, 1280−1282.

(12) Smith, E. L.; Abbott, A. P.; Ryder, K. S. Deep Eutectic Solvents (DESs) and Their Applications. *Chem. Rev.* **2014**, *114*, 11060−11082.

(13) Fedorov, M. V.; Kornyshev, A. A. Ionic Liquids at Electrified Interfaces. *Chem. Rev.* **2014**, *114*, 2978−3036.

(14) Garcia-Gomez, A.; Barranco, V.; Moreno-Fernandez, G.; Ibañez, J.; Centeno, T. A.; Rojo, J. M. Correlation between Capacitance and Porosity in Microporous Carbon Monoliths. *J. Phys. Chem. C* **2014**, *118*, 5134−5141.

(15) Forse, A. C.; Griffin, J. M.; Presser, V.; Gogotsi, Y.; Grey, C. P. Ring Current Effects: Factors Affecting the NMR Chemical Shift of Molecules Adsorbed on Porous Carbons. *J. Phys. Chem. C* **2014**, *118*, 7508−7514.

(16) Li, S.; Van Aken, K. L.; McDonough, J. K.; Feng, G.; Gogotsi, Y.; Cummings, P. T. The Electrical Double Layer of Dicationic Ionic Liquids at Onion-like Carbon Surface. *J. Phys. Chem. C* **2014**, *118*, 3901−3909.

(17) Uysal, A.; Zhou, H.; Feng, G.; Lee, S. S.; Li, S.; Fenter, P.; Cummings, P. T.; Fulvio, P. F.; Dai, S.; McDonough, J. K.; Gogotsi, Y. Structural Origins of Potential Dependent Hysteresis at the Electrified Graphene/Ionic Liquid Interface. *J. Phys. Chem. C* **2013**, *118*, 569−574.

(18) Vatamanu, J.; Hu, Z.; Bedrov, D.; Perez, C.; Gogotsi, Y. Increasing Energy Storage in Electrochemical Capacitors with Ionic Liquid Electrolytes and Nanostructured Carbon Electrodes. *J. Phys. Chem. Lett.* **2013**, *4*, 2829−2837.

(19) Qian, H.; Kucernak, A. R.; Greenhalgh, E. S.; Bismarck, A.; Shaffer, M. S. P. Multifunctional Structural Supercapacitor Composites Based on Carbon Aerogel Modified High Performance Carbon Fiber Fabric. *ACS Appl. Mater. Interfaces* **2013**, *5*, 6113−6122.

(20) Shi, K.; Ren, M.; Zhitomirsky, I. Activated Carbon-Coated Carbon Nanotubes for Energy Storage in Supercapacitors and Capacitive Water Purification. *ACS Sustain. Chem. Eng.* **2014**, *2*, 1289−1298.

(21) Xu, B.; Wu, F.; Chen, R.; Cao, G.; Chen, S.; Wang, G.; Yang, Y. Room Temperature Molten Salt as Electrolyte for Carbon Nanotube-Based Electric Double Layer Capacitors. *J. Power Sources* **2006**, *158*, 773−778.

(22) Chen, R.; Wu, F.; Liang, H.; Li, L.; Xu, B. Novel Binary Room-Temperature Complex Electrolytes Based on LiTFSI and Organic Compounds with Acylamino Group. *J. Electrochem. Soc.* **2005**, *152*, A1979−A1984.

DOI: 10.1021/jp5110455
J. Phys. Chem. C XXXX, XXX, XXX−XXX

(23) Boisset, A.; Jacquemin, J.; Anouti, M. Physical Properties of a New Deep Eutectic Solvent Based on Lithium Bis[(Trifluoromethyl)-Sulfonyl]Imide and *N*-Methylacetamide as Superionic Suitable Electrolyte for Lithium Ion Batteries and Electric Double Layer Capacitors. *Electrochim. Acta* **2013**, *102*, 120−126.

(24) Boisset, A.; Menne, S.; Jacquemin, J.; Balducci, A.; Anouti, M. Deep Eutectic Solvents Based on *N*-Methylacetamide and a Lithium Salt as Suitable Electrolytes for Lithium-Ion Batteries. *Phys. Chem. Chem. Phys.* **2013**, *15*, 20054−20063.

(25) Zaidi, W.; Timperman, L.; Anouti, M. Deep Eutectic Solvent Based on Sodium Cations as an Electrolyte for Supercapacitor Application. *RSC Adv.* **2014**, *4*, 45647−45652.

(26) Couadou, E.; Jacquemin, J.; Galiano, H.; Hardacre, C.; Anouti, M. A Comparative Study on the Thermophysical Properties for Two Bis[(trifluoromethyl)sulfonyl]imide-Based Ionic Liquids Containing the Trimethyl-Sulfonium or the Trimethyl-Ammonium Cation in Molecular Solvents. *J. Phys. Chem. B* **2013**, *117*, 1389−1402.

(27) Hu, Y.; Li, H.; Huang, X.; Chen, L. Novel Room Temperature Molten Salt Electrolyte Based on LiTFSI and Acetamide for Lithium Batteries. *Electrochem. Commun.* **2004**, *6*, 28−32.

(28) Anouti, M.; Timperman, L.; El Hilali, M.; Boisset, A.; Galiano, H. Sulfonium Bis(trifluorosulfonimide) Plastic Crystal Ionic Liquid as an Electrolyte at Elevated Temperature for High-Energy Supercapacitors. *J. Phys. Chem. C* **2012**, *116*, 9412−9418.

(29) Han, H.-B.; Nie, J.; Liu, K.; Li, W.-K.; Feng, W.-F.; Armand, M.; Matsumoto, H.; Zhou, Z.-B. Ionic Liquids and Plastic Crystals Based on Tertiary Sulfonium and Bis(fluorosulfonyl)imide. *Electrochim. Acta* **2010**, *55*, 1221−1226.

(30) Abbott, A. P.; Capper, G.; Gray, S. Design of Improved Deep Eutectic Solvents Using Hole Theory. *ChemPhysChem* **2006**, *7*, 803−806.

(31) Smith, J. A.; Webber, G. B.; Warr, G. G.; Atkin, R. Rheology of Protic Ionic Liquids and Their Mixtures. *J. Phys. Chem. B* **2013**, *117*, 13930−13935.

(32) Longinotti, M. P.; Corti, H. R. Fractional Walden Rule for Electrolytes in Supercooled Disaccharide Aqueous Solutions. *J. Phys. Chem. B* **2009**, *113*, 5500−5507.

(33) Breslau, B. R.; Miller, I. F. On the Viscosity of Concentrated Aqueous Electrolyte Solution. *J. Phys. Chem.* **1970**, *74*, 1056−1061.

(34) Dougassa, Y. R.; Jacquemin, J.; El Ouatani, L.; Tessier, C.; Anouti, M. Viscosity and Carbon Dioxide Solubility for $LiPF_6$, LiTFSI and LiFAP in Alkylcarbonates: Lithium Salt Nature and Concentration Effect. *J. Phys. Chem. B* **2014**, *118*, 3973−3980.

(35) Jones, G.; Dole, M. The Viscosity of Aqueous Solutions of Strong Electrolytes with Special Reference to Barium Chloride. *J. Am. Chem. Soc.* **1929**, *51*, 2950−2964.

(36) Chen, R.; Wu, F.; Li, L.; Xu, B.; Qiu, X.; Chen, S. Novel Binary Room-Temperature Complex System Based on LiTFSI and 2-Oxazolidinone and Its Characterization as Electrolyte. *J. Phys. Chem. C* **2007**, *111*, 5184−5194.

(37) Galinski, M.; Lewandowski, A.; Stepniak, I. Ionic Liquids as Electrolytes. *Electrochim. Acta* **2006**, *51*, 5567−5580.

(38) Abbott, A. P. Application of Hole Theory to the Viscosity of Ionic and Molecular Liquids. *ChemPhysChem* **2004**, *5*, 1242−1246.

(39) Okoturo, O. O.; VanderNoot, T. J. Temperature Dependence of Viscosity for Room Temperature Ionic Liquids. *J. Electroanal. Chem.* **2004**, *568*, 167−181.

(40) Xu, W.; Cooper, E. I.; Angell, C. A. Ionic Liquids: Ion Mobilities, Glass Temperatures, and Fragilities. *J. Phys. Chem. B* **2003**, *107*, 6170−6178.

(41) Yoshizawa, M.; Xu, W.; Angell, C. A. Ionic Liquids by Proton Transfer: Vapor Pressure, Conductivity, and the Relevance of Pka from Aqueous Solutions. *J. Am. Chem. Soc.* **2003**, *125*, 15411−15419.

(42) Pires, J.; Timperman, L.; Jacquemin, J.; Balducci, A.; Anouti, M. Density, Conductivity, Viscosity, and Excess Properties of (Pyrrolidinium Nitrate-Based Protic Ionic Liquid/Propylene Carbonate) Binary Mixture. *J. Chem. Thermodyn.* **2013**, *59*, 10−19.

(43) Portet, C.; Taberna, P. L.; Simon, P.; Laberty-Robert, C. Modification of Al Current Collector Surface by Sol−Gel Deposit for Carbon−Carbon Supercapacitor Applications. *Electrochim. Acta* **2004**, *49*, 905−912.

(44) Yasuda, T.; Nakamura, S.-i.; Honda, Y.; Kinugawa, K.; Lee, S.-Y.; Watanabe, M. Effects of Polymer Structure on Properties of Sulfonated Polyimide/Protic Ionic Liquid Composite Membranes for Non-humidified Fuel Cell Applications. *ACS Appl. Mater. Interfaces* **2012**, *4*, 1783−1790.

(45) Zhang, C.; Xie, Y.; Sun, G.; Pentecost, A.; Wang, J.; Qiao, W.; Ling, L.; Long, D.; Gogotsi, Y. Ion Intercalation into Graphitic Carbon with a Low Surface Area for High Energy Density Supercapacitors. *J. Electrochem. Soc.* **2014**, *161*, A1486−A1494.

DOI: 10.1021/jp5110455
J. Phys. Chem. C XXXX, XXX, XXX−XXX